
SignBot: Learning Human-to-Humanoid Sign Language Interaction

Guanren Qiao¹, Sixu Lin¹, Ronglai Zuo², Zhizheng Wu¹, Kui Jia^{1,3}, Guiliang Liu^{*1}

¹School of Data Science, The Chinese University of Hong Kong, Shenzhen,

²Imperial College, ³DexForce Technology

guanrenqiao1@link.cuhk.edu.cn, liuguiliang@cuhk.edu.cn,

Abstract

Sign language is a natural and visual form of language that uses movements and expressions to convey meaning, serving as a crucial means of communication for individuals who are deaf or hard-of-hearing (DHH). However, the number of people proficient in sign language remains limited, highlighting the need for technological advancements to bridge communication gaps and foster interactions with minorities. Based on recent advancements in embodied humanoid robots, we propose SignBot, a novel framework for human-robot sign language interaction. SignBot integrates a cerebellum-inspired motion control component and a cerebral-oriented module for comprehension and interaction. Specifically, SignBot consists of: 1) Motion Retargeting, which converts human sign language datasets into robot-compatible kinematics; 2) Motion Control, which leverages a learning-based paradigm to develop a robust humanoid control policy for tracking sign language gestures; and 3) Generative Interaction, which incorporates translator, responder, and generator of sign language, thereby enabling natural and effective communication between robots and humans. Simulation and real-world experimental results demonstrate that SignBot can effectively facilitate human-robot interaction and perform sign language motions with diverse robots and datasets. SignBot represents a significant advancement in automatic sign language interaction on embodied humanoid robot platforms, providing a promising solution to improve communication accessibility for the DHH community. Please refer to our webpage: <https://qiaoguanren.github.io/SignBot-demo/>

1 Introduction

Sign language, as the primary linguistic medium for the deaf and hard-of-hearing (DHH) communities, plays a vital role in bridging their communication barriers with other people. Recent advancements in computer vision and large language models (LLMs) have significantly enhanced sign language applications, including generation, translation, and recognition [1; 2; 3; 4; 5]. These advancements enable effective translation between sign language text, videos, and mesh representations. However, despite these advancements, their real-world impact on assisting individuals with disabilities remains limited. A key reason is that these systems are primarily demonstrated in virtual environments and cannot facilitate physical interaction with people in real-world scenarios.

To bridge this gap, the recent development of Embodied Artificial Intelligence (EAI), which integrates AI models into a physical form, offers a promising solution. Unlike traditional sign language generation or comprehension models, EAI emphasizes real-world interaction, task execution, and continuous learning through physical experiences [6]. Recent advancements in EAI have extended

*Corresponding author: Guiliang Liu, email: liuguiliang@cuhk.edu.cn

to the development of humanoid robots [7; 8], which, due to their human-like mechanical structure, can seamlessly integrate into human workspaces and living environments. These robots are capable of performing various daily tasks, such as housekeeping [9; 10; 11], cooking [12], and navigation [13; 14], making them a valuable platform for fostering natural physical interactions with humans.

Recent studies have explored learning-based perception and control algorithms, such as reinforcement learning (RL) [15; 16; 17] and imitation learning [18; 19], to develop control policies for humanoid robots. The commonly studied paradigms for learning-based methods include: 1) *Teleoperation* refers to the remote control of a humanoid robot by a human operator [11; 20; 21; 22; 23]. 2) *Command-based Control* means driving a humanoid robot with movement commands (e.g., velocity or affordance). Their control policies can be trained to imitate human behavioral norms [24; 16; 25; 26; 19]. However, no previous study has explored these methods for sign language applications. Teleoperation-based approaches typically rely on human manipulation, preventing robots from autonomously performing sign language, while command-based control methods primarily focus on the robot’s body without addressing the complexities of dexterous hand movements. Additionally, many dexterous robotic hands have limited degrees of freedom (DoFs), and the lack of wrist flexibility further restricts the accurate expression of the rich and diverse movements required for sign language.

To overcome this challenge, we introduce SignBot, an expressive robotic sign language framework designed for seamless interaction with sign language users. Our framework integrates an embodied cerebellum, which controls the balance and movements of a humanoid robot, and a generative cerebral that is responsible for comprehending received sign language and generating corresponding gestures for communication. SignBot mainly consists of three key components: 1) *Motion Retargeting*, which maps the action sequences from human sign language datasets into a format compatible with robotic kinematics [16; 27]. 2) *Policy Training (SignBot’s Cerebellum)*, which enables humanoid robots to first learn diverse sign language motions in a simulated environment with a decoupled policy [22; 23; 16]. Specifically, we utilize decoupled body policies to learn the entire sign language gesture. The upper body, including the hands, learns to track the target sign language poses through imitation learning, while the lower body maintains a stable standing posture using an RL policy. 3) *Sign Language Interaction (SignBot’s Cerebral)* integrates a sign language translator [28], a sign language responder [29], and a sign language generator [3], enabling the robot to understand user expressions and respond appropriately in sign language. To ensure stability while executing sign language gestures, we utilize a substantial amount of training data in the simulation to enhance its stability. By combining these elements, our framework enhances real-time human-robot interaction, bridging the communication gap between sign language users and embodied humanoid robot systems.

We design various experiments to verify the performance of SignBot under Goal-Tracking and Cumulative Rewards metrics and visualize the poses of humanoid robots performing sign language. Experimental results show that SignBot exhibits *accuracy*, *generalization*, *naturalness*, and *robustness* with various datasets and robots. Overall, the main contributions of our paper are as follows:

- (1) **Human-Robot Interaction for Minority.** We propose an interactive sign language framework that enables seamless communication between humanoid robots and the DHH community.
- (2) **Precise Sign Language Execution.** Our humanoid robot control policy robustly adapts to a diverse range of human sign language motions, ensuring stable and accurate execution.
- (3) **Embodiment and Domain Adaptation.** Our method can be transferred to different robots, achieving Sim-to-Real deployment and applying robot sign language in real interaction scenarios.

2 Related Work

Humanoid Robotic Imitation of Human Behavior. For the imitating human behavior problem of humanoid robots, researchers often adopt a whole-body control learning paradigm [7]. This paradigm consists mainly of two approaches. One approach is to decouple the upper and lower body policies, which are responsible for managing different parts of a humanoid robot. Representative works include Exbody [16], Mobile-Television [30], WoCoCo [31], OmniH2O [22], etc. Although upper and lower body policies are decoupled, they can still be integrated into a whole-body control paradigm. The alternative approach involves providing reference motions for the humanoid robot. Given the physical similarities to humans, a promising reference is the collection of human movements from motion datasets, such as H2O [20], Exbody2 [24], ASAP [25], UH-1 [32], [33], HiLo [34], HWC-Loco [35], etc. We simultaneously leverage the advantages of both methods to perform sign language. These reference motions provide rich signals for humanoid robots to imitate human-like motions.

Sign Language Processing. The field encompasses two primary research directions: sign language translation (SLT), and sign language generation (SLG). SLT and SLG form complementary pathways for bidirectional communication between deaf and hearing populations, specializing in sign-to-text and text-to-sign conversion, respectively [3]. Some studies successfully incorporated language models (LMs) pre-trained on extensive natural language corpora into SLT frameworks, yielding substantial accuracy enhancements [1; 5]. Recent state-of-the-art SLG works can be categorized into two classes: the first group of methods [36] employ diffusion models to generate sign motions conditioned on text inputs; the second group of methods [37; 4; 3] consider the linguistic nature of sign languages and adopts a tokenizer-LM autoregressive generation approach.

3 Problem Definition

Robot Learning Environment. We formulate the task of tracking human sign language motions as a Partially Observable Markov Decision Process (POMDP) defined by the tuple $\mathcal{M} = (\mathcal{O}, \mathcal{S}, \mathcal{A}, P_{\mathcal{T}}, \mathcal{R}, \mu_0, \gamma)$, where: 1) Within the observation space \mathcal{O} , each observation $o_t \in \mathcal{O}$ consists of two components: proprioception (o_t^p) and goal imitation (o_t^y). The proprioception o_t^p includes essential motion-related information such as the root state, joint positions, and joint velocities. Meanwhile, the goal imitation o_t^y represents a unified encoding of the whole-body sign language pose that must be tracked during reinforcement learning (RL) training. 2) $s_t \in \mathcal{S}$ records the complete information and environment of the robot. We summarize a state as $s_t = [o_t, o_{t-1}, \dots, o_{t-H}]$ and each $o_t = [o_t^p, o_t^y]$. 2) $a_t \in \mathcal{A}$ denotes the action space, and action $a \in \mathcal{A}$ denotes the target joint positions that a PD controller uses to actuate the DoF. 3) $r_t = \mathcal{R}(s_t, a_t)$ denotes the reward functions, which typically consist of penalty, regularization, and task rewards. These reward signals determine the level of optimality in the control policy, for which we provide a detailed introduction in Section 4.2. 4) $P_{\mathcal{T}} \in \Delta_{\mathcal{S} \times \mathcal{A}}^{\mathcal{S}}$ denotes the transition function as a mapping from state-action pairs to a distribution of future states. 5) $\mu_0 \in \Delta^{\mathcal{S}}$ denotes the initial state distribution. 6) $\gamma \in (0, 1]$ denotes the discounting factor. Under this POMDP, our goal is learning a control policy $\pi : \mathcal{S} \rightarrow \mathcal{A}$ that can maximize the discounted cumulative rewards $\sum_{t=0}^{T-1} \gamma^t r_t$. During the training process, we apply the PPO-based [38] algorithm to optimize the policy parameters: $\pi : \mathcal{S} \rightarrow \mathcal{A}$ where H is the length of history windows, intending to maximize the expected return of the discounted episode reward $J(\pi) = \mathbb{E}_{\pi} \left[\sum_{t=0}^{T-1} \gamma^t r_t \right]$, where T represents the length of the horizon of an episode. We learn the control policy via KL-regularized PPO [39; 40], and the optimized objective function can be defined as:

$$\mathbb{E}_t \left[\frac{\pi(a_t | s_t)}{\pi_{\text{old}}(a_t | s_t)} \hat{A}(s_t, a_t) + \alpha \mathcal{H}(\pi(s_t)) - \eta \text{KL}(\pi_{\text{old}}(s_t), \pi(s_t)) \right] \quad (1)$$

where $\hat{A}(s_t, a_t)$ denotes the estimated advantage function, $\mathcal{H}(\pi(s_t))$ denotes the entropy of policy and α, η are the regularization coefficients.

Human-Robot Sign Language Interaction. The problem of sign Language Interaction can be modelled as a closed-loop system. Firstly, the robot should observe a sequence of the user’s sign motions $\mathbf{o}^{\text{human}} = [o_1^{\text{human}}, \dots, o_K^{\text{human}}]$. Then, the robot translates sign language $\mathbf{o}^{\text{human}}$ into a sequence of text description $\mathbf{x} \sim \mathcal{X}$ (\mathcal{X} denotes the space of text sequence) with the translation function $f_{\mathcal{T}} : \mathcal{O}^K \rightarrow \mathcal{X}$. To respond, the system must understand the intention of \mathbf{x}_t and answer \mathbf{x}'_t with the responding function $f_{\mathcal{R}} : \mathcal{X} \rightarrow \mathcal{X}$. Based on the text response \mathbf{x}'_t , the system should generate sign language $\mathbf{o}_t^{\text{robot}}$ with the generation function $f_{\mathcal{G}} : \mathcal{X} \rightarrow \mathcal{O}^K$, which can be used as imitation goals for robot controller. Specifically, we formulate the sign language generation problem as a conditional sequence generation task, where the goal is to generate a sign language SMPL-X sequence from input semantic information. The output sign language sequence \mathbf{o}^y is the SMPL-X representation space of sign language and K denotes the length of the motion sequence. Typically, this is modeled by the conditional probability distribution $P_{\mathcal{G}}(\mathbf{o}^y | \mathbf{x}) = \prod_{k=1}^K P_{\mathcal{G}}(o_k^y | \mathbf{o}_{<k}^y, \mathbf{x})$.

4 SignBot

In this section, we introduce the pipeline of SignBot, which is divided into three parts: 1) **Motion Retargeting** of the body and hands, 2) **Policy Training** to control the robot’s movements as “SignBot’s cerebellum”, and 3) **Sign Language Reasoning** for comprehensive and responding users’ sign languages as “SignBot’s cerebral” [41]. Figure 1 presents the pipeline of SignBot.

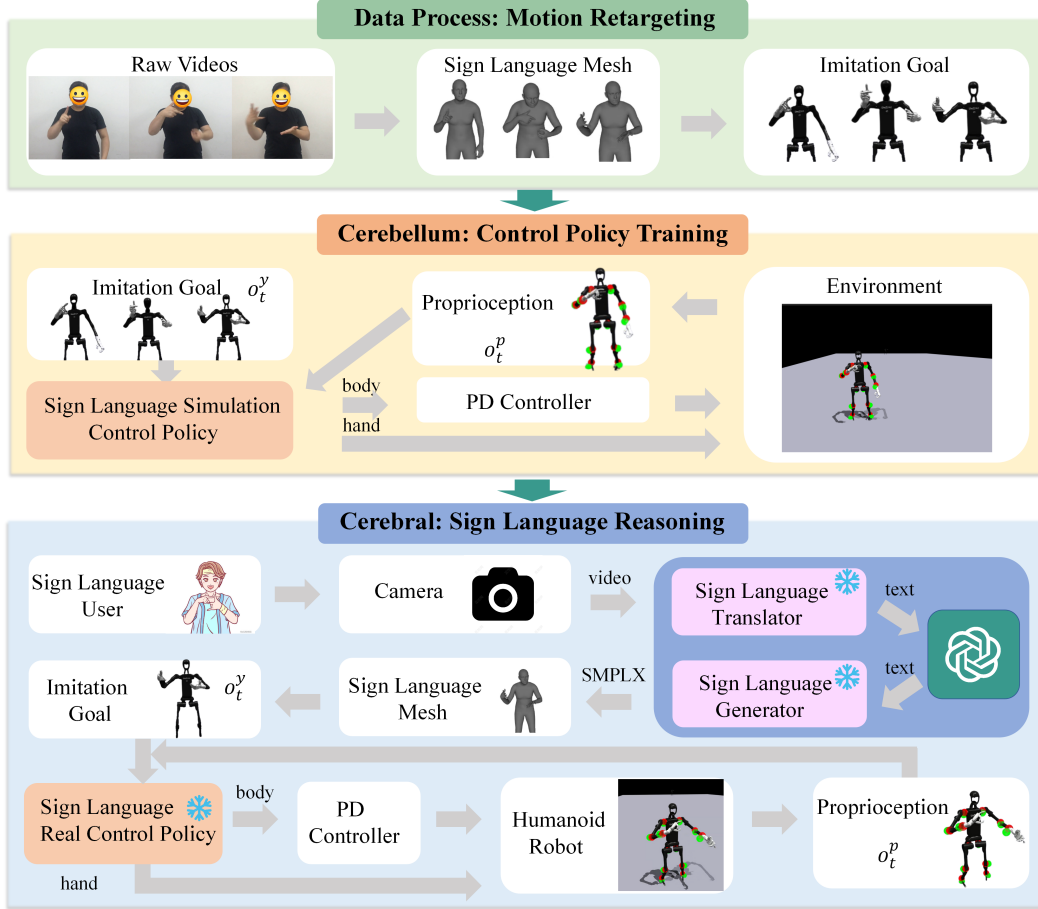


Figure 1: Overview of SignBot: The framework consists of three stages: (1) *Motion Retargeting* aligns human sign language gestures with the body structure of humanoid robots (Section 4.1). (2) *Cerebellum* performs Sim2Real policy training that enables the robot to track various sign language gestures in the simulated environment and deploy the policy to real-world (Section 4.2). (3) *Cerebral* conducts sign language reasoning to facilitate communication with sign language users through the sign language translator, response, and generator within the cerebral (Section 4.3).

4.1 Motion Retargeting

As shown in the first stage of Figure 1, we extract the motion from the video mesh for subsequent data processing. To mitigate differences in body shape between humans and the humanoid robot, we perform retargeting separately for the human body and hands.

Body Retargeting. Our humanoid body retargeting system is based on an improved version of [42]. By establishing a mapping relationship between the source keypoints and the target keypoints, we design a dual T-Pose (the standard poses of the source and target skeletons) as a spatial alignment reference. We convert the local quaternion of each joint to the form of axis angles. Then the mapped angle is presented: $\mathbf{m} = \beta \mathbf{a}$, where $\mathbf{m} = [q_i, q_j, q_k]$ corresponds to the degrees of freedom in local quaternion, β denotes the rotation angle, and $\mathbf{a} = [a_x, a_y, a_z]$ is the rotation axis. For 1D joints (the elbow, torso, knee, and ankle), we take the rotation angle projected onto the corresponding rotation axis of the 1D joints. It is important to note that to make the robot’s sign language movements more natural, we add two additional degrees of freedom at the robot’s wrist and transform the wrists and shoulders represented by a 1D joint to a 3D joint. As shown in Figure 1, the retargeted humanoid motion data retains critical sign language characteristics, including gesture accuracy and expressiveness under our hardware system.

Hand Retargeting. To map human hand pose data to the joint positions of the Linker hand (the robot hands used by SignBot), we apply the preprocessing method from [27], adapting it specifically for the Linker hand. This process is often formulated as an optimization problem [43], where the difference

between the keypoint vectors of the human hand model and the dexterous hand is minimized. Due to the misaligned DoFs in the fingers of the linker hand with the human hand model, we properly freeze several finger joints. Since the linker hand is larger than a typical dexterous hand, we adjust the scale factor in the optimization process. Additionally, we modify the regularization term to smooth the sign language movements between consecutive frames.

4.2 SignBot’s Cerebellar: Control Policy Training

Within our SignBot humanoid agent, the cerebellum controls the low-level movements for performing sign language. As shown in the second stage of Figure 1, we train a motion control policy to enable the humanoid robot to track and imitate sign language gestures in a simulated environment. In this section, we discuss our approach from three key perspectives: observation space, decoupled policy, and reward design.

Observation Space. SignBot’s observation $o_t \in \mathcal{O}$ consists of proprioception (o_t^p) and goal imitation (o_t^y) (Section 3). Our proprioception is defined as $o_t^p \triangleq [\mathbf{q}_t, \dot{\mathbf{q}}_t, \mathbf{v}_t, \mathbf{w}_t, \mathbf{g}_t, \mathbf{a}_{t-1}]$, which includes joint position $\mathbf{q}_t \in \mathbb{R}^{55}$ (DoF position), joint velocity $\dot{\mathbf{q}}_t \in \mathbb{R}^{55}$ (DoF velocity), root linear velocity $\mathbf{v}_t \in \mathbb{R}^3$, root angular velocity $\mathbf{w}_t \in \mathbb{R}^3$, root projected gravity $\mathbf{g}_t \in \mathbb{R}^3$, and the previous action $\mathbf{a}_{t-1} \in \mathbb{R}^{55}$. The goal observation is $o_t^y \triangleq [\hat{\mathbf{q}}^{kp}, \hat{\mathbf{q}}, \dot{\hat{\mathbf{q}}}]$, where $\hat{\mathbf{q}}^{kp} \in \mathbb{R}^{14 \times 3}$ are the positions of 14 selected reference keypoints [16] to ensure that the humanoid robot and the imitation goal are oriented in the same direction, $\hat{\mathbf{q}} \in \mathbb{R}^{55 \times 3}$ are the positions of all reference joints, and $\dot{\hat{\mathbf{q}}}$ is the linear velocity of the reference joints. At the same time, we generally perform domain randomization [22; 20] in the simulation environment to ensure robustness and generalization. Appendix B.3 summarizes the domain randomization terms that we have utilized in SignBot.

Decoupled Policy. Given that sign language involves precise coordination of both hand poses and full-body motion with high DoFs, learning a unified control policy is inherently challenging. More importantly, while the dual arms in the upper body can often be governed by a shared control strategy, the control approach for the lower body may vary significantly depending on the physical design of the humanoid robot. For instance, bipedal humanoid robots typically utilize reinforcement learning (RL) controller, whereas wheeled robots often employ model predictive control (MPC) techniques.

Motivated by recent advances in whole-body humanoid control [16; 30], we adopt a decoupled architecture that separates the control policies of the upper and lower body. The primary objective of the upper-body policy π^{upper} is to track the retargeted actions, while the lower-body policy π^{lower} ensures balance in the robot’s default standing pose while adapting to the movements of π^{upper} .

$$\begin{aligned} \pi^{upper} &= \arg \min_{\pi} \mathbb{E}_{(s, a_*^{up})} \left[\mathcal{D}_f[\delta(a_*^{up}) \| \pi(a^{up} | s)] \right] \\ \pi^{lower} &= \arg \max_{\pi} \mathbb{E}_{\pi(a^{low} | s)} \left[\sum_{t=0}^{\infty} \gamma^t r_t(s, a) | a^{lower} \sim \pi^{upper} \right] \end{aligned} \quad (2)$$

Where: 1) a_*^{up} represents the retargeted action of the upper body, and δ denotes the Dirac delta function. 2) $\mathcal{D}_f(\cdot \| \cdot)$ refers to the f -divergence (e.g., KL-divergence) between two distributions. 3) The whole-body humanoid action, $a = [a^{low}, a^{up}]$, is the concatenation of upper and lower body actions. 4) The reward from the humanoid control learning environment can be represented by the weighted penalty $r_{\mathfrak{P}}$, task $r_{\mathfrak{T}}$, and regularization $r_{\mathfrak{R}}$ terms [23]: $r_t = \beta_{\mathfrak{T}} r_{\mathfrak{T}} + \beta_{\mathfrak{P}} r_{\mathfrak{P}} + \beta_{\mathfrak{R}} r_{\mathfrak{R}}$. In our task, task rewards ($r_{\mathfrak{T}}$) measure the robot’s performance in tracking joint motions and body velocities. Penalty rewards ($r_{\mathfrak{P}}$) serve to discourage undesirable outcomes such as falling and violating dynamic constraints like joint or torque limits. Regularization rewards ($r_{\mathfrak{R}}$) are used to align the humanoid’s sign language gestures with human preferences. Appendix B specifies the reward functions.

Note that to train the lower-body policy π^{lower} , we apply the PPO [38] algorithm for leggy humanoid robots and MPC for wheeled humanoid robots. In this way, SignBot can be scaled to multiple embodiments, for which we demonstrate in the experiment.

4.3 SignBot’s Cerebral: Sign Language Reasoning

Within our SignBot humanoid agent, the cerebral system controls high-level reasoning skills, enabling it to respond sign language and generate appropriate responses. An ideal embodied humanoid robot needs to have both cerebellar and cerebral capabilities, enabling it to interact effectively with its surrounding environment and other agents. The third stage of Figure 1 illustrates the cerebral system

of the SignBot humanoid robot. This system processes the user’s input and generates an appropriate sign language response, which serves as the imitation goal for the control policy (\mathbf{o}_t^c in Section 4.2).

Implementation. SignBot utilizes a camera to observe the motions of sign language users and then stores this as a video input into its cerebral system. For communicating with sign language users in real-time, SignBot’s cerebral system is implemented by three models: a *sign language translator* understanding sign language contents, a *sign language responder* interpreting semantics and generating responses, and a *sign language generator* converting texts to the SMPLX format with Transformer-based models. We introduce these two models in the following:

Sign Language Translator is implemented with a LLM [28]. In the pre-training stage, it extracts the sign language features from sign language videos and images, aligns them with the dimensions of the language model, and then inputs them into the model. In the fine-tuning stage, we utilize the translation text of the sign language dataset [44; 45; 46] to construct the supervised label for fine-tuning our translation model.

Sign Language Responder is implemented using the DeepSeek-R1 API [29] due to its ability to seamlessly comprehend semantic information and facilitate multi-turn conversations. To simulate natural conversations with sign language users, we design a suitable prompt template. When generating a response, the system integrates the text-format sign language into the prompt and produces a contextually appropriate reply. A prompt example can be seen in Appendix D.1.

Sign Language Generator autoregressively generates 3D sign motions from text input using a pretrained multilingual LM [47]. Firstly, we design a decoupled VQVAE tokenizer to map continuous sign motions into discrete tokens over upper body (UB), left hand (LH), and right hand (RH) movements [48; 49]. Given a K -frame sign sequence, we decompose it into three part-wise motion sequences based on the SMPL-X format: $\mathbf{C}^u \in \mathbb{R}^K$, where $u \in \{\text{UB}, \text{LH}, \text{RH}\}$. For each body part, we train a separate VQ-VAE comprising an encoder that projects the sequence into a latent space $\mathbf{C}_{f_{enc}}^u = \{c_{f,k}^u\}_{k=1}^K \in \mathbb{R}^{K_{f_{enc}} \times C}$, a decoder for reconstruction, and a learnable codebook $\mathbf{Z}_u \in \mathbb{R}^{N_Z^u \times d}$, where N_Z^u represents the number of codes and d denotes the code dimension. Then, for each pose, we can derive a set of discrete tokens $\hat{\mathbf{z}}_{1,\dots,K}^u = [\hat{z}_1^u, \dots, \hat{z}_K^u]$, which searches for the nearest neighbor from the codebook \mathbf{Z}_u :

$$\hat{z}_k^u = \arg \min_{z_n \in \mathbf{Z}_u} \|s_{f_{enc},k}^u - z_n\|^2, \quad n \in [1, N_Z^u], \quad \forall u \in \{\text{UB}, \text{LH}, \text{RH}\} \quad (3)$$

Given a text description \mathbf{x} , the generator retrieves word-level signs based on the \mathbf{x} from external dictionaries made by the decoupled tokenizer [3]. These word-level signs are represented with discrete tokens $\hat{\mathbf{z}}_{1,\dots,K}^u$. We feed these tokens and text sequence \mathbf{x} into the LM encoder at the same time. During decoding, we adopt a multi-head decoding strategy [3]. We design three language modeling heads, implemented as fully connected layers, to predict motion tokens for each body part from m simultaneously at each step. The decoding process can be formulated as:

$$P_{Dec}(\mathbf{o}^y | \mathbf{h}) = \prod_{k=1}^K \prod_u P_{Dec}(o_k^y | \mathbf{o}_{<k}^{y,\mathbf{h}}) = \prod_{k=1}^K P_{Dec}(o_k^{y,\text{UB}} | \mathbf{o}_{<k}^{y,\mathbf{h}}) P_{Dec}(o_k^{y,\text{LH}} | \mathbf{o}_{<k}^{y,\mathbf{h}}) P_{Dec}(o_k^{y,\text{RH}} | \mathbf{o}_{<k}^{y,\mathbf{h}}) \quad (4)$$

where $(\mathbf{o}_{<k}^y, \mathbf{h})$ is the simplification of $\mathbf{o}_{<k}^{y,\mathbf{h}}$, $\mathbf{o}^y = \{o_1^{y,\text{UB}}, o_1^{y,\text{LH}}, o_1^{y,\text{RH}}, \dots, o_K^{y,\text{UB}}, o_K^{y,\text{LH}}, o_K^{y,\text{RH}}\}$ and $\mathbf{h} = f_{\text{Enc}}(\mathbf{x}, \hat{\mathbf{z}}_{1,\dots,K}^u)$ denotes the output of LM Encoder. Finally, the derived motion tokens are used to reconstruct sign motions. The training objective is to maximize the log-likelihood $\sum_{(\mathbf{x}, \mathbf{o}^y) \in \mathcal{D}} \log P_{\mathcal{G}}(\mathbf{o}^y | \mathbf{x}) = \sum_{(\mathbf{x}, \mathbf{o}^y) \in \mathcal{D}} P_{Dec}(\mathbf{o}^y | f_{\text{Enc}}(\mathbf{x}, \hat{\mathbf{z}}_{1,\dots,K}^u))$ over datasets \mathcal{D} .

The imitation goal produced by the generator corresponds to the sign language poses that the humanoid robot must perform. By using these poses (\mathbf{o}_t^y in Section 4.2) to guide the control policy, users can interact effectively with SignBot in sign language.

Sim2Real Deployment. In real-world environments, robot movement from positions from t to $t + 1$ is not instantaneous. To ensure smooth transitions, we employ the Ruckig algorithm [50] for online trajectory generation with third-order (jerk) constraints and complete kinematic targets. Ruckig computes time-optimal trajectories between arbitrary states, defined by position, velocity, and acceleration, while respecting velocity, acceleration, and jerk limits. To maintain smooth motion, we interpolate intermediate values between target positions. For safety during deployment, we avoid commanding joint angles near their physical limits, as slight discrepancies between simulation and reality may lead to motor power loss or low-voltage issues, even when using identical limit settings.

5 Environment

Experiment Settings. To conduct a comprehensive evaluation, we quantify the performance of SignBot in simulated (IssacGym [51]) and realistic environments from the following perspectives: 1) *Accuracy*: How to effectively align sign language actions between robots and humans? 2) *Generalization*: How well does SignBot perform with diverse sign language datasets and different robots? 3) *Naturalness*: How effectively does SignBot imitate human-like sign language norms in the real-world interaction scenarios? We employ consistent evaluation metrics across all environments. These metrics include 1) *Tracking DoF Pos Error* tracks the errors of the demonstrations’ degree of freedom position. 2) *Tracking Yaw* tracks the error of the body yaw angle. 3) *Tracking Linear Velocity* tracks the error of the intrinsic linear velocity. 4) *Tracking Roll&Pitch*: tracks the errors of the body roll&pitch angle. 5) *Cumulative Rewards*: are calculated by all the weighted reward functions. We use the publicly available CSL-Daily Chinese Sign Language dataset [44] and the How2Sign American Sign Language dataset [46] as experimental training data. Our experiments are conducted *across different embodiments*. We utilize legged robots H1, wheeled robots W1, and Linker hand to verify our methods. Appendix A records details of our experimental setting.

Comparison Methods. To demonstrate the effectiveness of SignBot, we compare with other baselines based on whole-body control or RL as follows: 1) **SignBot (w/o Lower-Body Tracking)** follows SignBot, but allows the lower body to self-adapt and maintain balance. 2) **Whole-Body Tracking + AMP** like [19] uses an AMP reward [42; 52] to encourage the transitions of the policy to be similar to the motions of the sign language features. 3) **Whole-Body Tracking** like [20] learns the movement of the upper body and lower body simultaneously. Appendix B reports the detailed parameter settings.

5.1 Accuracy: Alignment of Sign Language between Human and Robot

Precise execution of sign language is vital for effective communication within the DHH community, as even minor inaccuracies can lead to misunderstandings, in contrast to boxing techniques, where approximate gesture replication suffices for demonstration purposes. We divide the CSL-Daily sign language dataset [44] into three difficulty levels according to the length of the sentences: simple (929 sentences), intermediate (4558 sentences), and difficult (1089 sentences). The levels of difficulty increase with the length of the evaluated sentence. We compare SignBot with previously mentioned baselines on the data across these three difficulty levels. Appendix B records the running details of this experiment.

Baseline \ Metric	DoF Pos ↓	Yaw ↓	Linear Velocity ↓	Roll&Pitch ↓	Cumulative Rewards ↑
Easy					
Whole-Body Tracking	0.97 ± 0.01	0.16 ± 0.01	0.18 ± 0.01	0.05 ± 0.00	10.41 ± 0.70
Whole-Body Tracking + AMP	1.13 ± 0.01	0.11 ± 0.00	0.22 ± 0.00	0.04 ± 0.01	8.89 ± 0.32
SignBot (w/o Lower-Body Tracking)	0.85 ± 0.01	0.95 ± 0.01	1.86 ± 0.02	0.26 ± 0.01	0.54 ± 0.01
SignBot	0.59 ± 0.01	0.04 ± 0.00	0.20 ± 0.01	0.03 ± 0.01	12.46 ± 0.40
Medium					
Whole-Body Tracking	0.95 ± 0.01	0.17 ± 0.00	0.17 ± 0.01	0.05 ± 0.00	10.63 ± 0.63
Whole-Body Tracking + AMP	1.12 ± 0.01	0.10 ± 0.00	0.22 ± 0.00	0.04 ± 0.00	9.18 ± 0.32
SignBot (w/o Lower-Body Tracking)	0.87 ± 0.01	0.97 ± 0.00	1.87 ± 0.02	0.27 ± 0.01	0.33 ± 0.01
SignBot	0.61 ± 0.00	0.08 ± 0.00	0.20 ± 0.01	0.04 ± 0.01	12.24 ± 0.57
Hard					
Whole-Body Tracking	0.94 ± 0.01	0.17 ± 0.00	0.17 ± 0.01	0.05 ± 0.00	9.67 ± 0.20
Whole-Body Tracking + AMP	1.11 ± 0.02	0.10 ± 0.00	0.23 ± 0.01	0.04 ± 0.01	9.04 ± 0.24
SignBot (w/o Lower-Body Tracking)	0.85 ± 0.00	0.92 ± 0.01	2.00 ± 0.02	0.04 ± 0.00	0.52 ± 0.03
SignBot	0.59 ± 0.01	0.04 ± 0.00	0.20 ± 0.03	0.03 ± 0.01	12.56 ± 0.30

Table 1: Tracking Performance: We compare model performance under three difficulty levels. The mean ± std results for each baseline are shown in the dataset under the three random seeds. Bolded results indicate the best performance. The rewards calculation denotes the cumulative returns over a trajectory, while the other metrics are calculated using the mean square error.

Table 1 illustrates the training performance of each baseline under different difficulty levels. The results indicate that SignBot achieves the lowest error in metrics such as DoF position tracking and yaw angle tracking, while also achieving the highest reward value, demonstrating the effectiveness of the SignBot control policy. The improvement in tracking accuracy and the reduction in training difficulty are attributed to the provision of upper body DoF position data and the tracking of lower body bent standing position. SignBot excels in controlling yaw and roll&pitch angles, indicating strong stability of the robot base. We also test other baselines, such as tracking the upper and whole body DoF positions, but the performance of these is unsatisfactory. This is because sign language

differs from other upper-body movements; it is flexible and varied, and the frequency of sign language actions in the dataset is relatively fast. In addition, we observe that the length of the sentences does not significantly affect SignBot’s performance. When the sentences are short, SignBot tends to have larger errors in tracking keypoints. This may be due to the shorter episode length, which causes the robot to complete and reset its random learning for the next action quickly. During this period, it needs to adjust the robot’s global pose frequently. We also provide a more intuitive case study to compare various baselines (See Appendix C). Please see more video examples.

5.2 Generalization: Imitation across diverse datasets and robots

Generalizing SignBot to different embodiments. We retarget the human sign language data to align with the joints of humanoid robots to visualize the precision in imitating sign language poses.

Notably, since the Unitree H1’s wrist has only one DoF, it can only rotate while maintaining a fixed orientation and cannot bend. To address this, we modify the robot by adding two additional DoFs to the wrist, which allows the wrist to move up/down and left/right, enabling more flexible sign language gestures. Figures 2 and 3 illustrate the alignment between human and robot sign language gestures after applying our SignBot method, demonstrated on both the legged Unitree H1 and the wheeled W1 robots. A notable observation is that SignBot maintains a high accuracy in imitating sign language across both robots. In particular, balancing is challenging for legged humanoid robots. To address this, we design a reward function that encourages both stability and accurate imitation of upper-body movements. By combining this reward formulation with our SignBot, the RL controller enables the robot (**red joint**) to track demonstration motions (**green joint**).

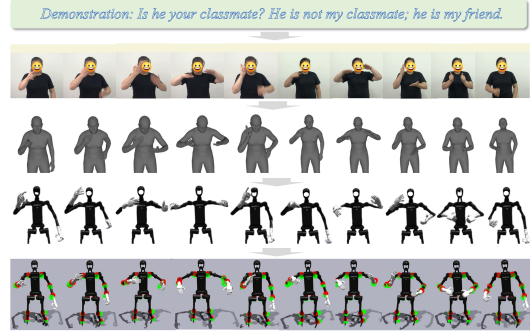


Figure 2: Sign Language Alignment between Human and Robots: We display the source video of human sign language in the first row, followed by the mesh from video processing, then the re-targeted sign language demonstration on the SignBot, and the last row shows the result after training in Isaac Gym. In the last row, the **red** nodes represent the joints of the SignBot, while the **green** nodes represent the targetted demonstration nodes.

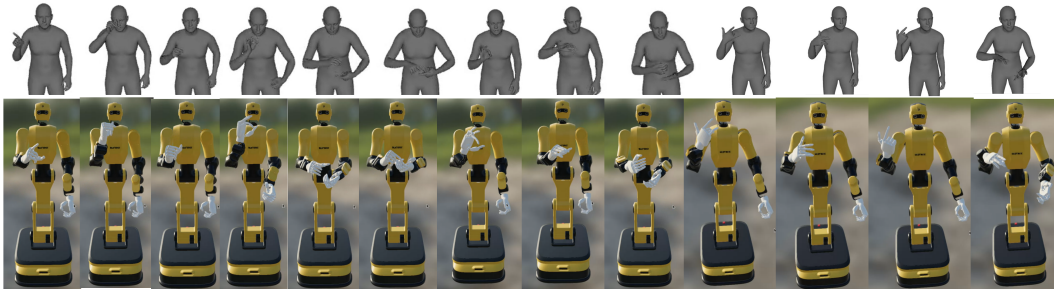


Figure 3: Sign Language Alignment between Human and Wheeled Robot.

Generalizing SignBot to different Datasets. To demonstrate the generalization capability of SignBot, we evaluate SignBot with another English sign language dataset.

Specifically, we preprocess a portion of the 2,286 data entries from the How2Sign dataset [46] and evaluate the robustness of the policy for different sign languages following Table 1. Table 2 illustrates SignBot’s performance on the How2Sign dataset, demonstrating that SignBot achieves a minimal tracking error while maintaining high rewards.

Baseline	Metric			
	DoF Pos ↓	Yaw ↓	Linear Velocity ↓	Roll&Pitch ↓
	Easy			
Whole-Body Tracking	1.05 ± 0.02	0.32 ± 0.00	0.16 ± 0.01	0.04 ± 0.00
SignBot	0.63 ± 0.02	0.07 ± 0.02	0.19 ± 0.03	0.07 ± 0.01
	Medium			
Whole-Body Tracking	0.88 ± 0.02	0.34 ± 0.01	0.15 ± 0.02	0.04 ± 0.01
SignBot	0.57 ± 0.02	0.11 ± 0.01	0.17 ± 0.02	0.05 ± 0.00
	Hard			
Whole-Body Tracking	0.90 ± 0.03	0.30 ± 0.03	0.17 ± 0.02	0.05 ± 0.01
SignBot	0.56 ± 0.01	0.11 ± 0.02	0.18 ± 0.02	0.05 ± 0.01

Table 2: Generalization Experiment.

5.3 Naturalness: Sim-to-Real Human-Robot Interaction

To demonstrate the naturalness of SignBot, we demonstrate its performance in realistic environments. To deploy SignBot on the H1 robot, we must add a pair of wrists and an intermediary connection between the wrists and the arm. We find updating the hardware system challenging. To prevent hardware limitations, we conduct the real-world experiment on the Linker Hand and the W1 robot. The W1 robot and Linker Hand are controlled through the ROS system to drive the various joints during real deployment.

Figure 4 illustrates several examples of interactions between sign language users and a robot functioning as a supermarket cashier. In these scenarios, the robot initiates communication by asking customers about their intended purchases. As is typical in retail environments, the robot promotes the distinctive qualities of the products, such as the freshness of the fruits, to encourage customer engagement and stimulate sales. Subsequently, the robot addresses pricing inquiries by estimating realistic, everyday prices in its responses. Throughout these human-robot interactions, the robot exhibits a high degree of accuracy in executing critical sign language gestures, including pointing forward, giving a thumbs-up, and performing the "OK" sign. While occasional delays may occur, primarily for reasoning purposes or to ensure adherence to path planning constraints, the control policy ensures that each joint reaches its designated position along the planned trajectory. Due to space constraints, we are unable to present additional examples within the paper; however, further instances can be found in the supplementary video materials and Appendix D.

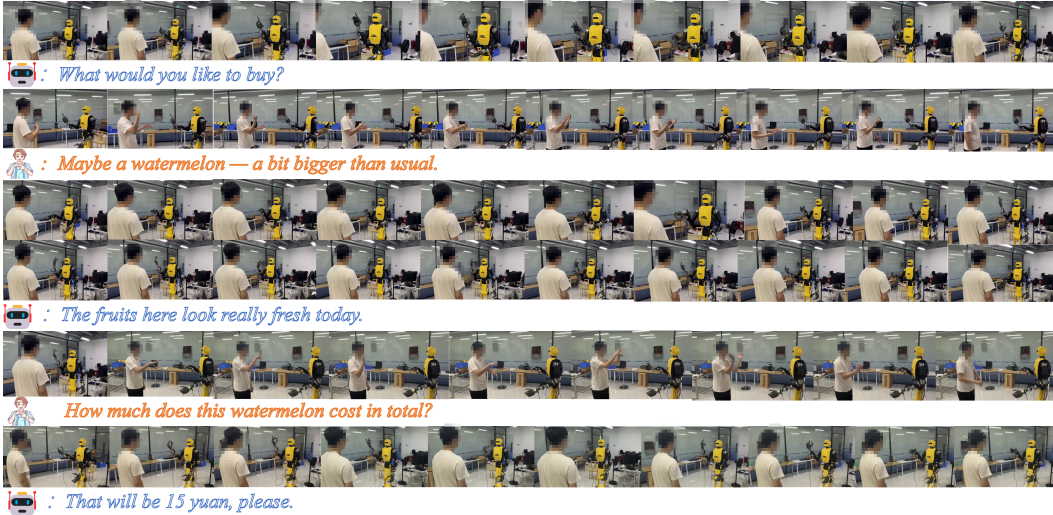


Figure 4: An example of real-world interaction between the robot and the human customer.

Limitation. 1) *Limitations in Sign Language Translation.* Current state-of-the-art open-source models for sign language translation still exhibit errors, making it difficult to handle complex expressions. Although not the primary focus of this work, more advanced models can be seamlessly integrated into our framework in the future. 2) *Latency in Human-Robot Interaction.* The robot’s reasoning module currently relies on separate models for dialogue, translation, and sign language generation, resulting in latency. Unifying these components into a vision-language-action model that directly produces robot-adapted sign language actions could greatly improve real-time performance.

6 Conclusion

We introduce SignBot, a human-robot sign language interaction framework for humanoid robots that incorporates an embodied cerebellum + cerebral cooperation mechanism. This framework has been validated across various sign language motions, demonstrating exceptional accuracy, generalization, naturalness, and adaptability across diverse sign language scenarios. In particular, the cerebellum + cerebral cooperation mechanism in SignBot achieves reliable performance in daily communication through the sign language translator, response, and generator. We think SignBot is a foundational solution for sign language applications, such as daily sign language robots serving the DHH community. A promising direction for future research is integrating SignBot with manipulation skills. In this way, we can not only communicate with the DHH community but also assist them in completing tasks.

References

- [1] Ryan Wong, Necati Cihan Camgoz, and Richard Bowden. Sign2gpt: Leveraging large language models for gloss-free sign language translation. In *International Conference on Learning Representations, (ICLR)*, 2024.
- [2] Yutong Chen, Fangyun Wei, Xiao Sun, Zhirong Wu, and Stephen Lin. A simple multi-modality transfer learning baseline for sign language translation. In *Proceedings of the IEEE/CVF Conference on Computer Vision and Pattern Recognition, (CVPR)*, pages 5120–5130, 2022.
- [3] Ronglai Zuo, Rolandos Alexandros Potamias, Evangelos Ververas, Jiankang Deng, and Stefanos Zafeiriou. Signs as tokens: An autoregressive multilingual sign language generator. *arXiv preprint arXiv:2411.17799*, 2024.
- [4] Zhengdi Yu, Shaoli Huang, Yongkang Cheng, and Tolga Birdal. Signavatars: A large-scale 3d sign language holistic motion dataset and benchmark. In *European Conference on Computer Vision (ECCV)*, pages 1–19, 2024.
- [5] Peiqi Jiao, Yuecong Min, and Xilin Chen. Visual alignment pre-training for sign language translation. In *European Conference on Computer Vision, (ECCV)*, 2024.
- [6] Agrim Gupta, Silvio Savarese, Surya Ganguli, and Li Fei-Fei. Embodied intelligence via learning and evolution. *Nature communications*, 12(1):5721, 2021.
- [7] Zhaoyuan Gu, Junheng Li, Wenlan Shen, Wenhao Yu, Zhaoming Xie, Stephen McCrory, Xianyi Cheng, Abdulaziz Shamsah, Robert Griffin, C. Karen Liu, Abderrahmane Kheddar, Xue Bin Peng, Yuke Zhu, Guanya Shi, Quan Nguyen, Gordon Cheng, Huijun Gao, and Ye Zhao. Humanoid locomotion and manipulation: Current progress and challenges in control, planning, and learning. *arXiv preprint arXiv:2501.02116*, 2025.
- [8] Giuseppe Paolo, Jonas Gonzalez-Billandon, and Balázs Kégl. Position: a call for embodied ai. In *Forty-first International Conference on Machine Learning, (ICML)*, 2024.
- [9] Xavier Puig, Eric Undersander, Andrew Szot, Mikael Dallaire Cote, Tsung-Yen Yang, Ruslan Partsey, Ruta Desai, Alexander William Clegg, Michal Hlavac, So Yeon Min, et al. Habitat 3.0: A co-habitat for humans, avatars and robots. *arXiv preprint arXiv:2310.13724*, 2023.
- [10] Yufei Wang, Zhou Xian, Feng Chen, Tsun-Hsuan Wang, Yian Wang, Katerina Fragkiadaki, Zackory Erickson, David Held, and Chuang Gan. Robogen: Towards unleashing infinite data for automated robot learning via generative simulation. *arXiv preprint arXiv:2311.01455*, 2023.
- [11] Zipeng Fu, Qingqing Zhao, Qi Wu, Gordon Wetzstein, and Chelsea Finn. Humanplus: Humanoid shadowing and imitation from humans. *Conference on Robot Learning, (CoRL)*, 2024.
- [12] Soroush Nasiriany, Abhiram Maddukuri, Lance Zhang, Adeet Parikh, Aaron Lo, Abhishek Joshi, Ajay Mandlekar, and Yuke Zhu. Robocasa: Large-scale simulation of everyday tasks for generalist robots. *arXiv preprint arXiv:2406.02523*, 2024.
- [13] Hanqing Wang, Wei Liang, Luc Van Gool, and Wenguan Wang. Dreamwalker: Mental planning for continuous vision-language navigation. In *Proceedings of the IEEE/CVF international conference on computer vision, (ICCV)*, pages 10873–10883, 2023.
- [14] Sheng Fan, Rui Liu, Wenguan Wang, and Yi Yang. Navigation instruction generation with bev perception and large language models. In *European Conference on Computer Vision, (ECCV)*, pages 368–387, 2024.
- [15] Richard S Sutton. Reinforcement learning: An introduction. *A Bradford Book*, 2018.
- [16] Xuxin Cheng, Yandong Ji, Junming Chen, Ruihan Yang, Ge Yang, and Xiaolong Wang. Expressive whole-body control for humanoid robots. In *Proceedings of Robotics: Science and Systems, (RSS)*, 2024.
- [17] Guanren Qiao, Guorui Quan, Rongxiao Qu, and Guiliang Liu. Modelling competitive behaviors in autonomous driving under generative world model. In *European Conference on Computer Vision, (ECCV)*, pages 19–36. Springer, 2024.

- [18] Annan Tang, Takuma Hiraoka, Naoki Hiraoka, Fan Shi, Kento Kawaharazuka, Kunio Kojima, Kei Okada, and Masayuki Inaba. Humanmimic: Learning natural locomotion and transitions for humanoid robot via wasserstein adversarial imitation. In *IEEE International Conference on Robotics and Automation, (ICRA)*, 2024.
- [19] Honghao Liao, Zhiheng Li, Ziyu Meng, Ran Song, Yibin Li, and Wei Zhang. Integrating controllable motion skills from demonstrations. *arXiv preprint arXiv:2408.03018*, 2024.
- [20] Tairan He, Zhengyi Luo, Wenli Xiao, Chong Zhang, Kris Kitani, Changliu Liu, and Guanya Shi. Learning human-to-humanoid real-time whole-body teleoperation. *IEEE/RSJ International Conference on Intelligent Robots and Systems, (IROS)*, 2024.
- [21] Xuxin Cheng, Jialong Li, Shiqi Yang, Ge Yang, and Xiaolong Wang. Open-television: Teleoperation with immersive active visual feedback. *arXiv preprint arXiv:2407.01512*, 2024.
- [22] Tairan He, Zhengyi Luo, Xialin He, Wenli Xiao, Chong Zhang, Weinan Zhang, Kris Kitani, Changliu Liu, and Guanya Shi. Omnih2o: Universal and dexterous human-to-humanoid whole-body teleoperation and learning. In *Conference on Robot Learning, (CoRL)*, 2024.
- [23] Zipeng Fu, Tony Z. Zhao, and Chelsea Finn. Mobile aloha: Learning bimanual mobile manipulation with low-cost whole-body teleoperation. In *Conference on Robot Learning, (CoRL)*, 2024.
- [24] Mazeyu Ji, Xuanbin Peng, Fangchen Liu, Jialong Li, Ge Yang, Xuxin Cheng, and Xiaolong Wang. Exbody2: Advanced expressive humanoid whole-body control. *arXiv preprint arXiv:2412.13196*, 2024.
- [25] Tairan He, Jiawei Gao, Wenli Xiao, Yuanhang Zhang, Zi Wang, Jiashun Wang, Zhengyi Luo, Guanqi He, Nikhil Sobanbab, Chaoyi Pan, et al. Asap: Aligning simulation and real-world physics for learning agile humanoid whole-body skills. *arXiv preprint arXiv:2502.01143*, 2025.
- [26] Tairan He, Wenli Xiao, Toru Lin, Zhengyi Luo, Zhenjia Xu, Zhenyu Jiang, Jan Kautz, Changliu Liu, Guanya Shi, Xiaolong Wang, et al. Hover: Versatile neural whole-body controller for humanoid robots. *arXiv preprint arXiv:2410.21229*, 2024.
- [27] Yuzhe Qin, Wei Yang, Binghao Huang, Karl Van Wyk, Hao Su, Xiaolong Wang, Yu-Wei Chao, and Dieter Fox. Anyteleop: A general vision-based dexterous robot arm-hand teleoperation system. In *Robotics: Science and Systems, (RSS)*, 2023.
- [28] Zecheng Li, Wengang Zhou, Weichao Zhao, Kepeng Wu, Hezhen Hu, and Houqiang Li. Uni-sign: Toward unified sign language understanding at scale. *International Conference on Learning Representations, (ICLR)*, 2025.
- [29] Daya Guo DeepSeek-AI, Dejian Yang, Haowei Zhang, Junxiao Song, Ruoyu Zhang, Runxin Xu, Qihao Zhu, Shirong Ma, Peiyi Wang, Xiao Bi, et al. Deepseek-r1: Incentivizing reasoning capability in llms via reinforcement learning. *arXiv preprint arXiv:2501.12948*, 2025.
- [30] Chenhao Lu, Xuxin Cheng, Jialong Li, Shiqi Yang, Mazeyu Ji, Chengjing Yuan, Ge Yang, Sha Yi, and Xiaolong Wang. Mobile-television: Predictive motion priors for humanoid whole-body control. *arXiv preprint arXiv:2412.07773*, 2024.
- [31] Chong Zhang, Wenli Xiao, Tairan He, and Guanya Shi. Wococo: Learning whole-body humanoid control with sequential contacts. In *Conference on Robot Learning, (CoRL)*, 2024.
- [32] Jiageng Mao, Siheng Zhao, Siqi Song, Tianheng Shi, Junjie Ye, Mingtong Zhang, Haoran Geng, Jitendra Malik, Vitor Guizilini, and Yue Wang. Learning from massive human videos for universal humanoid pose control. *arXiv preprint arXiv:2412.14172*, 2024.
- [33] Qiang Zhang, Peter Cui, David Yan, Jingkai Sun, Yiqun Duan, Gang Han, Wen Zhao, Weining Zhang, Yijie Guo, Arthur Zhang, et al. Whole-body humanoid robot locomotion with human reference. In *IEEE/RSJ International Conference on Intelligent Robots and Systems, (IROS)*, 2024.

- [34] Qiyuan Zhang, Chenfan Weng, Guanwu Li, Fulai He, and Yusheng Cai. Hilo: Learning whole-body human-like locomotion with motion tracking controller. *arXiv preprint arXiv:2502.03122*, 2025.
- [35] Sixu Lin, Guanren Qiao, Yunxin Tai, Ang Li, Kui Jia, and Guiliang Liu. Hwc-loco: A hierarchical whole-body control approach to robust humanoid locomotion. *arXiv preprint arXiv:2503.00923*, 2025.
- [36] Vasileios Baltatzis, Rolandos Alexandros Potamias, Evangelos Ververas, Guanxiong Sun, Jiankang Deng, and Stefanos Zafeiriou. Neural sign actors: A diffusion model for 3d sign language production from text. In *Proceedings of the IEEE/CVF Conference on Computer Vision and Pattern Recognition, (CVPR)*, pages 1985–1995, 2024.
- [37] Aoxiong Yin, Haoyuan Li, Kai Shen, Siliang Tang, and Yueting Zhuang. T2s-gpt: Dynamic vector quantization for autoregressive sign language production from text. In *Association for Computational Linguistics, (ACL)*, 2024.
- [38] John Schulman, Filip Wolski, Prafulla Dhariwal, Alec Radford, and Oleg Klimov. Proximal policy optimization algorithms. *arXiv preprint arXiv:1707.06347*, 2017.
- [39] John Schulman, Filip Wolski, Prafulla Dhariwal, Alec Radford, and Oleg Klimov. Proximal policy optimization algorithms. *CoRR*, abs/1707.06347, 2017.
- [40] Guanren Qiao, Guiliang Liu, Pascal Poupart, and Zhiqiang Xu. Multi-modal inverse constrained reinforcement learning from a mixture of demonstrations. *Advances in Neural Information Processing Systems, (NeurIPS)*, 36:60384–60396, 2023.
- [41] Yang Liu, Weixing Chen, Yongjie Bai, Guanbin Li, Wen Gao, and Liang Lin. Aligning cyber space with physical world: A comprehensive survey on embodied ai. *arXiv preprint arXiv:2407.06886*, 2024.
- [42] Xue Bin Peng, Yunrong Guo, Lina Halper, Sergey Levine, and Sanja Fidler. Ase: Large-scale reusable adversarial skill embeddings for physically simulated characters. *ACM Transactions On Graphics (TOG)*, 41(4):1–17, 2022.
- [43] Ankur Handa, Karl Van Wyk, Wei Yang, Jacky Liang, Yu-Wei Chao, Qian Wan, Stan Birchfield, Nathan Ratliff, and Dieter Fox. Dexpilot: Vision-based teleoperation of dexterous robotic hand-arm system. In *IEEE International Conference on Robotics and Automation, (ICRA)*, pages 9164–9170, 2020.
- [44] Hao Zhou, Wengang Zhou, Weizhen Qi, Junfu Pu, and Houqiang Li. Improving sign language translation with monolingual data by sign back-translation. In *Proceedings of the IEEE/CVF Conference on Computer Vision and Pattern Recognition, (CVPR)*, 2021.
- [45] Hezhen Hu, Weichao Zhao, Wengang Zhou, and Houqiang Li. Signbert+: Hand-model-aware self-supervised pre-training for sign language understanding. *IEEE Transactions on Pattern Analysis and Machine Intelligence (TPAMI)*, pages 1–20, 2023.
- [46] Amanda Duarte, Shruti Palaskar, Lucas Ventura, Deepti Ghadiyaram, Kenneth DeHaan, Florian Metze, Jordi Torres, and Xavier Giro-i Nieto. How2sign: a large-scale multimodal dataset for continuous american sign language. In *Proceedings of the IEEE/CVF conference on computer vision and pattern recognition, (CVPR)*, pages 2735–2744, 2021.
- [47] Yinhan Liu, Jiatao Gu, Naman Goyal, Xian Li, Sergey Edunov, Marjan Ghazvininejad, Mike Lewis, and Luke Zettlemoyer. Multilingual denoising pre-training for neural machine translation. *Transactions of the Association for Computational Linguistics*, 8:726–742, 2020.
- [48] Aaron Van Den Oord, Oriol Vinyals, et al. Neural discrete representation learning. *Advances in neural information processing systems, (NeurIPS)*, 30, 2017.
- [49] Shunlin Lu, Ling-Hao Chen, Ailing Zeng, Jing Lin, Ruimao Zhang, Lei Zhang, and Heung-Yeung Shum. Humantomato: Text-aligned whole-body motion generation. In *International Conference on Machine Learning, (ICML)*, 2024.

- [50] Lars Berscheid and Torsten Kröger. Jerk-limited real-time trajectory generation with arbitrary target states. *Robotics: Science and Systems XVII, (RSS)*, 2021.
- [51] Viktor Makoviychuk, Lukasz Wawrzyniak, Yunrong Guo, Michelle Lu, Kier Storey, Miles Macklin, David Hoeller, Nikita Rudin, Arthur Allshire, Ankur Handa, et al. Isaac gym: High performance gpu-based physics simulation for robot learning. *arXiv preprint arXiv:2108.10470*, 2021.
- [52] Jonathan Ho and Stefano Ermon. Generative adversarial imitation learning. *Advances in neural information processing systems, (NeurIPS)*, 29, 2016.
- [53] Georgios Pavlakos, Vasileios Choutas, Nima Ghorbani, Timo Bolkart, Ahmed A. A. Osman, Dimitrios Tzionas, and Michael J. Black. Expressive body capture: 3d hands, face, and body from a single image. In *Proceedings IEEE Conf. on Computer Vision and Pattern Recognition, (CVPR)*, 2019.

A. Experiment Preparation

This section mainly introduces the simulation platform we used, the humanoid robot, the dexterous hand, and the Chinese sign language dataset. Figure 5 shows the platform and robotic equipment used in our experiments.

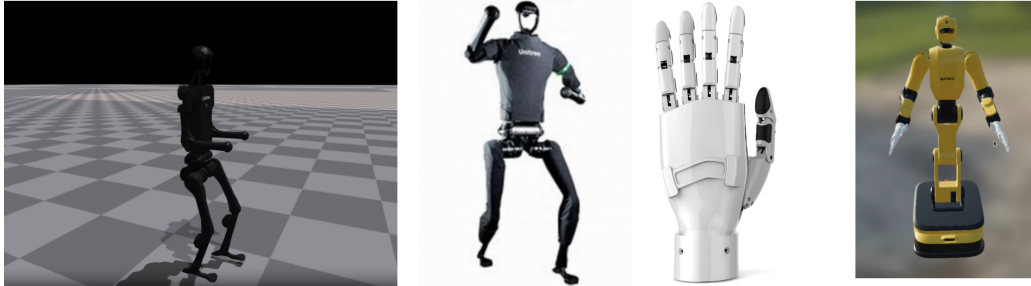


Figure 5: Experiment Preparation: The above shows the environment for loading the H1/W1 robot in IsaacGym, with the H1/W1 robot in the lower left and the Linker hand dexterous hand in the lower right.

A.1. Experiment Platform

IsaacGym is a high-performance robotics simulation and reinforcement learning training platform based on the PhysX physics engine and GPU parallel computing technology. It supports real-time simulation of tens of thousands of robot instances running simultaneously on a single GPU. The platform is optimized for research in robot control, motion planning, and reinforcement learning, providing a native Python interface and an extensible API that allows developers to efficiently train complex policies (such as bipedal robot gaits and robotic arm grasping). Its core advantage lies in its massive parallelization capability, significantly accelerating training efficiency by offloading physics computations to the GPU, and it is widely used in research and development in fields such as industrial automation and human-robot interaction.

A.2. Experiment Equipment

Unitree H1: is a full-size general-purpose humanoid robot, weighing approximately 47 kg and standing around 180 cm tall, matching the physical dimensions of an average adult. Its body boasts 19 degrees of freedom (DoF), with bio-inspired joint designs in the legs and high-performance motors. The system is capable of integrating reinforcement learning algorithms to achieve real-time environmental mapping and disturbance-resistant balance control, while also supporting future integration with LLMs to enhance interactive capabilities.

Linker Hand dexterous hand product has a maximum of 42 degrees of freedom, successfully simulating the fine movements of the human hand. With its 360-degree rotation capability, we have integrated the Linker Hand into humanoid robots to enable them to perform a wider range of tasks in future research work.

W1 Robot The W1 stands 170 cm tall and is equipped with 34 advanced power units, providing strong and stable power support for the robot’s operation, ensuring precise and accurate coordination across all functions. Each power unit has a communication bandwidth of up to 100 Mbps. In terms of motion control, the W1 achieves an impressive control frequency of 1000 times per second. It is equipped with a 7-degree-of-freedom humanoid robotic arm, with a maximum single-arm load capacity of 10 kg, sufficient to handle various heavy load tasks. Additionally, the repeat positioning accuracy can be controlled within a precise range of ± 0.5 mm. The W1 is also equipped with dual cameras and binocular visual recognition algorithms, which can be used for perception tasks.

CSL-Daily Dataset is a large-scale continuous Chinese sign language dataset aimed at promoting research and applications in sign language recognition, translation, and generation technologies. This dataset contains over 20,000 sign language videos recorded by 10 sign language users, covering daily life scenarios including family life, school life, and healthcare. Each video is captured using high-definition cameras from various angles with synchronized collection, and each video is meticulously annotated with text. We create a word cloud (see Figure 6) to help readers better understand this dataset.



Figure 6: CSL-Daily Dataset WordCloud Figure.

Parametric Human Model The SMPLX model [53] based on the SMPL extends parametric human representations with expressive capabilities for body, hands, and face. SMPLX parameterizes the human form through body shape parameters $\beta \in \mathbb{R}^{10}$, joint pose parameters $\theta \in \mathbb{R}^{55 \times 3}$, and global translation $p \in \mathbb{R}^3$. The SMPLX function $\mathcal{S}(\beta, \theta, p) : \beta, \theta, p \rightarrow \mathbb{R}^{10475 \times 3}$ maps these parameters to the 3D coordinates of a high-fidelity mesh with 10,475 vertices.

B. Training Details

This section mainly introduces some of the environment parameters and algorithm parameters we used. During training, we also made special adjustments to certain joints. For example, we do not track the ankle joint to avoid restricting the H1’s flexibility in adjusting its position. Additionally, we slightly bent the knee joint to ensure greater stability.

B.1. Task, Regularization and Penalty Rewards

B.2. PPO Parameters

We apply PPO to train the H1 robot. Table 4 shows the PPO parameters.

B.3. Domain Randomization

Domain randomization is implemented across all training environments. This technique introduces variability in various environmental parameters, including friction and gravity. Detailed specifications of the domain randomization can be found in Table 5.

B.4. Running Setting

To eliminate redundancy caused by the same sign language data being demonstrated by different users, we remove duplicate samples and select the 6576 sign language data for training baselines.

Term	Expression	Weight
Task Reward		
DoF position	$\exp(-0.7 \hat{\mathbf{q}}_t - \mathbf{q}_t)$	6.0
Keypoint position	$\exp(- \hat{\mathbf{q}}_t - \mathbf{q}_t)$	5.0
Body linear velocity	$\exp(-4.0 \hat{\mathbf{v}}_t - \mathbf{v}_t)$	6.0
Body Roll	$\exp(- \hat{R}_t - R_t)$	1.0
Body Pitch	$\exp(- \hat{P}_t - P_t)$	1.0
Body Yaw	$\exp(- \hat{Y}_t - Y_t)$	1.0
Penalty Reward		
DoF pos limit	$1(\mathbf{q}_t \notin [\mathbf{q}_{\min}, \mathbf{q}_{\max}])$	$-1e^{-2}$
Alive	1	1
Regularization Reward		
Time in Air	$\sum_i t_i^{air} * 1^{new\ contact}$	10.0
Drag	$\sum_i \ \mathbf{v}_{foot}\ * 1^{new\ contact}$	-0.1
Contact Force	$1\{ F_t^i \geq F_{th}\} * (F_t^i - F_{th})$	-3e-3
Stumble	$1\{\exists i, F_{xy}^i > 4 F_z^i \}$	-2.0
DoF Acceleration	$ \dot{\mathbf{q}} ^2$	-3e-7
Action Rate	$ \mathbf{a}_t - \mathbf{a}_r $	-1e-1
Energy	$ \dot{\mathbf{q}} ^2$	-1e-3
DoF Limit Violation	$1\{\mathbf{q}_i > \mathbf{q}_{max} \mid \mathbf{q}_i < \mathbf{q}_{min}\}$	-10.0
DoF Deviation	$\ \mathbf{q}_{ie}^{low} - \mathbf{q}^{low}\ ^2$	-1e-1
Vertical Linear Velocity	v_z	-1.0
Horizontal Angular Velocity	$\ \omega_{xy}\ ^2$	-0.4
Projected Gravity	$\ \mathbf{g}_{xy}\ ^2$	-2.0

Table 3: Task, Penalty and regularization reward expressions for different terms.

Table 4: PPO Hyperparameters

Hyperparameter	Value
Discount Factor	0.99
GAE Parameter	0.95
Timesteps per Rollout	21
Epochs per Rollout	5
Minibatches per Epoch	4
Entropy Bonus	0.01
Value Loss Coefficient	1.0
Clip Range	0.2
Reward Normalization	yes
Learning Rate	1e-3
Optimizer	Adam

We run experiments with three different seeds and present the mean \pm std results for each algorithm. To ensure a fair comparison, we maintain the same settings for all comparison baselines. We use 123, 321, and 1 as the experimental seeds, and we present the mean \pm standard deviation (std) for each evaluated algorithm. The training process for the motion control policy utilizes 12GB of GPU memory across 1 RTX 4090 and typically runs around 48 hours.

B.5. Torque Setting

The PD gains, characterized by stiffness and damping values, used in the IssacGym simulator are detailed in Table 6.

C. Case Study

We conduct a case study (see Figure 7), and it can be observed that while whole-body tracking provides relatively stable tracking of the lower body, the upper body exists some errors due to its inability to keep up with the motion frequency. Additionally, if SignBot does not track the posture of the lower body, it becomes very difficult to maintain stability. In addition, because our H1 robot has a pair of larger dexterous hands and a pair of modified wrists, the weight of the upper body has increased. Employing upper body tracking/whole body tracking methods makes it difficult for the robot to maintain its center of gravity while standing still. Therefore, we decouple the policy to allow RL to primarily learn to track the lower body, reducing the difficulty of training.

Figure 8 shows the interaction between human and H1 robot.

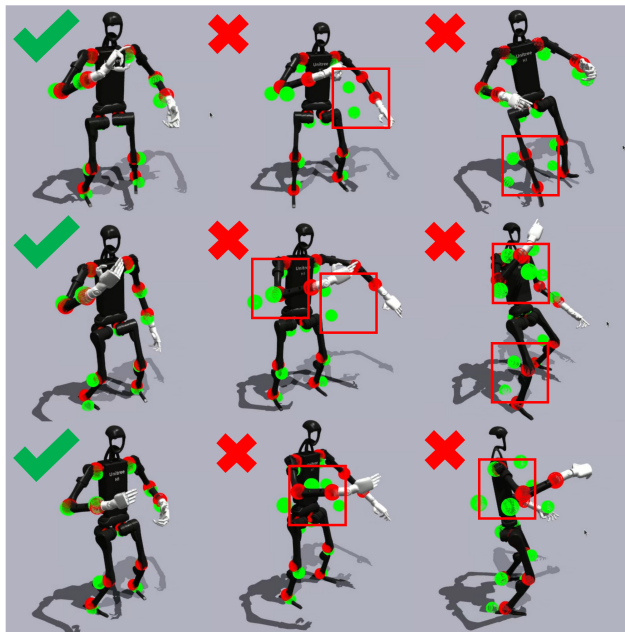


Figure 7: From left to right: SignBot, Whole-body tracking, and SignBot (w/o Lower-Body Tracking).

Term	Value
Dynamics Randomization	
Friction	$\mathcal{U}(0.6, 2)$
Base CoM offset	$\mathcal{U}(-0.07, 0.07)\text{m}$
Base Mass offset	$\mathcal{U}(-1, 5)\text{kg}$
Motor Strength	$\mathcal{U}(0.8, 1.2) \times \text{default}$
Gravity	$\mathcal{U}(-0.1, 0.1)$
Link Mass offset	$\mathcal{U}(0.7, 1.3)\text{kg}$
PD Gains	$\mathcal{U}(0.75, 1.25) \times \text{default}$
External Perturbation	
Push robot	interval = 8s, $v_{xy} = 0.3\text{m/s}$

Table 5: Domain randomization parameters: we include the friction, gravity, motor strength, base CoM/mass offset of torso link, link mass, PD Gains and an external perturbation.

D. Sign Language Interaction Experiment Supplement

D.1. Prompt

The sign language responder needs a suitable prompt template, which mainly depends on your scenario. We briefly provide a template for family life, and you can also encourage it to ask you questions or interact. In experiments, it may sometimes produce some strange responses, so it is occasionally necessary to guide the LLM and set word limits.

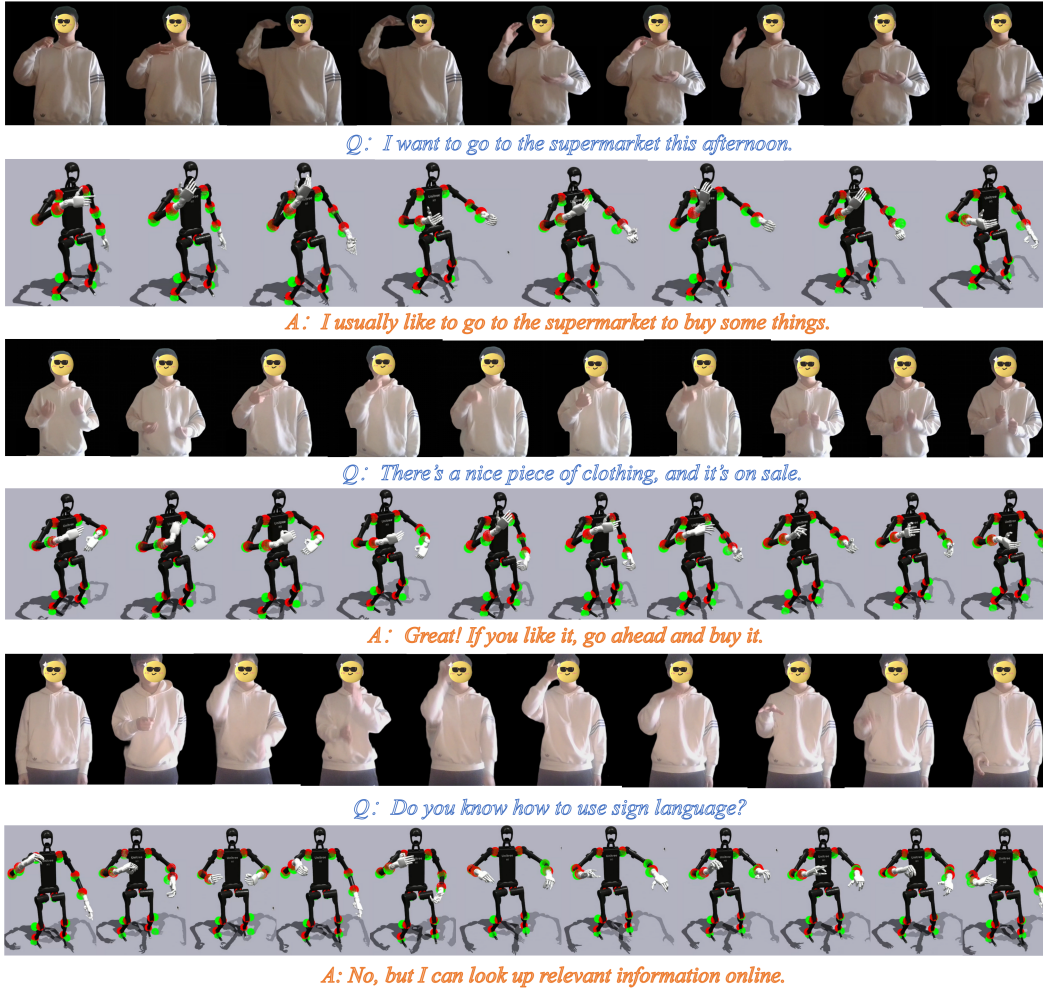


Figure 8: Sign Language Alignment between Human and Legged Robot.

Table 6: Torque Parameters

Joint Names	Stiffness [N-m/rad]	Damping [N-m-s/rad]	Torque Limit [Nm]
hip yaw	200	5	170
hip roll	200	5	170
hip pitch	200	5	170
knee	300	6	255
ankle	40	2	34
torso	200	5	170
shoulder	30	2	34
elbow	30	2	18
hand	30	2	18

Please act as a family member in daily life, such as my siblings. The topics can include greetings, family, work, food, travel, etc. Responses should be concise, reasonable, and logical according to everyday life. You can interact appropriately by asking reasonable questions or providing sensible answers based on what I say, and the responses should not be lengthy. Your response should think and speculate about the meaning of what the other person is saying as much like a human as possible, and answer using everyday logic. For example, if someone invites you to run together and you want to join, you need to have some reasonable basis, such as you enjoy running or you believe running is beneficial for your health. If you don't want to run with them, it might be because you're not feeling well, or you have other important matters to attend to, such as studying, or due to external reasons like bad weather today.

D.2 More Expressive Interaction Examples

Please check Figure 8. Even without the H1 hardware, we can attempt sign language interaction tasks in simulation.